Electronic Supplementary Material (ESI) for Materials Chemistry Frontiers.


# Supporting Information

**Multiplying electroluminescent efficiencies of red TADF emitters via a regioisomeric approach of the donor unit**

Xi Zhang,[a] Hui Wang,[a] Jia-Xiong Chen,[b] Lu Zhou,[a] Xiao-Yao Hao,[a] Jia Yu,[a] Kai Wang*[a,c] and Xiao-Hong Zhang*[a,d]

[a] Institute of Functional Nano & Soft Materials (FUNSOM), Soochow University, Suzhou, Jiangsu 215123, P. R. China

[b] School of Chemical Engineering and Light Industry, Guangdong University of Technology, Guangzhou, Guangdong, 510006, P.R. China

[c] Jiangsu Key Laboratory for Carbon-Based Functional Materials & Devices, Soochow University, Suzhou, 215123, Jiangsu, PR China

[d] Jiangsu Key Laboratory of Advanced Negative Carbon Technologies, Soochow University, Suzhou, 215123, Jiangsu, PR China

*E-mail: wkai@suda.edu.cn, xiaohong_zhang@suda.edu.cn

**General Information**

All reagents and starting materials were obtained from commercial suppliers and used without further purification. NMR spectra were recorded by a Bruker 400 spectrometer at room temperature, and mass spectra were recorded on a Thermo ISQ mass spectrometer using a direct exposure probe. TGA and DSC measurements were performed using a TAQ 500 thermogravimeter and DSC1 differential scanning calorimeter, respectively. UV–vis absorption spectra were recorded on a Hitachi U-3900 spectrophotometer. PL spectra and phosphorescent spectra were recorded on a Hitachi F-4600 fluorescence spectrophotometer. PL quantum yields and transient PL decay were measured using an Edinburgh Instruments FLS980 spectrometer under vacuum. Cyclic voltammetry (CV) was carried out on a CHI660E electrochemical analyzer, and the Ag/AgCl electrode and the Pt disk were used as the reference and working electrodes, respectively. In addition, 0.1 M tetrabutylammonium hexafluorophosphate ($TBAPF_6$) in $10^{-3}$ M dichloromethane solution served as the supporting electrolyte with ferrocene/ferrocenium ($Fc/Fc^{+}$) as the internal reference. The experiments were carried out under a nitrogen atmosphere at a scan rate of 0.05 V $s^{-1}$. The energy levels of HOMO ($E_{HOMO}$) and LUMO ($E_{LUMO}$) of the compounds are determined from the onsets of their oxidation and reduction curves in $10^{-3}$ M DCM solution relative to that of Fc+/Fc by using the equations $E_{HOMO}$ [eV] = $-(E_{ox}- E_{1/2, Fc} + 5.1)$ eV and $E_{LUMO}$ [eV] = $-(E_{re}- E_{1/2, Fc} + 5.1)$ eV.

**Theoretical calculations**

All the calculations were performed based on the Gaussian 09 program package. Theoretical calculations of the ground states and the excited states are performed by using density functional theory (DFT) and time-dependent DFT (TD-DFT) at the level of B3LPY/6-31G (*d*), respectively.

**Device fabrication and measurement**

OLEDs were fabricated on indium-tin oxide (ITO)-coated transparent glass substrates, and the ITO conductive layer had a thickness of ca. 100 nm and a sheet resistance of ca. 30 Ω per square. The substrates were cleaned with deionized water, acetone and ethanol, dried in an oven, and finally exposed to UV ozone for 15 min. All organic materials and metal layers were thermally evaporated under a vacuum of ca. $10^{-5}$ Torr. Four identical OLED devices were formed on each of the substrates, and the emission area was 0.1 $cm^2$ for each device. The deposition rates and thicknesses of all materials were monitored with oscillating quartz crystals. The deposition rates for organic materials, LiF, and Al were controlled at 1-2, 0.1, and 4-6 Å $s^{-1}$, respectively. The EL performances of the devices were measured with a PHOTO RESEARCH Spectra Scan PR 655 PHOTOMETER and a KEITHLEY 2400 Source Meter constant current source at room temperature.

**Single-crystal structure**

The corresponding CCDC reference numbers (CCDC: 2263082 for DPDPZ-PXZPh and 2262759 for DPDPZ-PhPXZ) and the data can be obtained free of charge from the Cambridge Crystallographic Data Centre via www.ccdc.cam.ac.uk/data_request/cif.

## Experimental

### Synthetic Methods

The intermediates M1 and M2 were synthesized according to previous reports.[1] Other chemicals and reagents used in this work were purchased commercially without further purification.

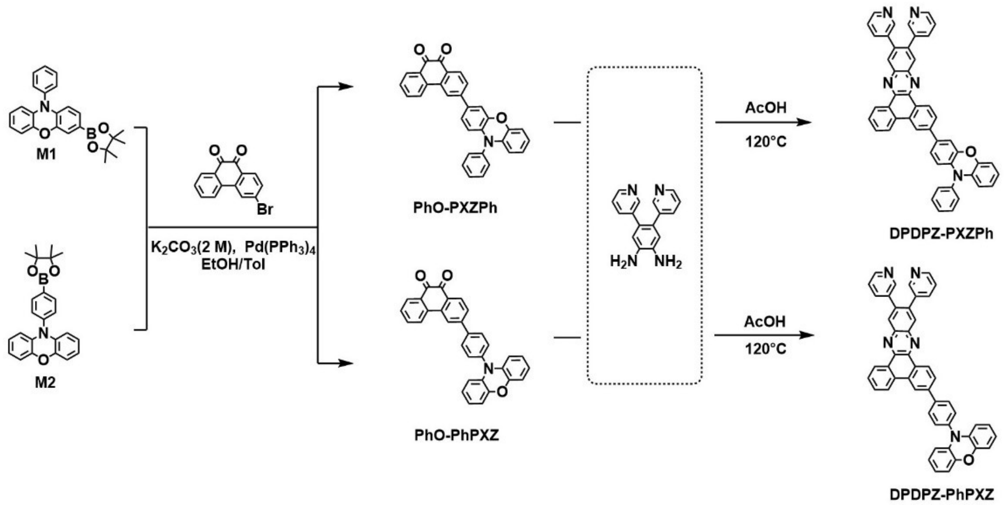


**Scheme S1.** Synthetic routes of DPDPZ-PXZPh and DPDPZ-PhPXZ.

**Synthesis of 3-(10-phenyl-10*H*-phenoxazin-3-yl)phenanthrene-9,10-dione (PhO-PXZPh)**. M1 (1.15 g, 3 mmol), 3-bromophenanthrene-9,10-dione (947 mg, 3.3 mmol), $K_2CO_3$ (3 mL, 2 M), $Pd(PPh_3)_4$ (104 mg, 0.09 mmol), 30 mL EtOH and 90 mL toluene were added into a three-necked flask (250 mL) under a nitrogen atmosphere. Then, the mixture was stirred at 100 °C for 24 h. After the reaction was completed, dichloromethane and water were added, and the organic layer was separated and concentrated in vacuo. The residue solid was purified by column chromatography to obtain the product (1.02 g, 73%). $^1$H NMR (400 MHz, Chloroform-d, δ) 8.18 (dd, $J$ = 7.7, 4.6 Hz, 2H), 8.07 (d, $J$ = 5.9 Hz, 2H), 7.72 (t, $J$ = 6.9 Hz, 1H), 7.64 (t, $J$ = 7.6 Hz, 2H), 7.55-7.50 (m, 2H), 7.47 (t, $J$ = 7.5 Hz, 1H), 7.38 (d, $J$ = 7.0 Hz, 2H), 7.05 (d, $J$ = 2.1 Hz, 1H), 6.96 (dd, $J$ = 8.4, 2.2 Hz, 1H), 6.73-6.67 (m, 2H), 6.63 (td, $J$ = 7.4, 6.9, 2.2 Hz, 1H), 6.01 (d, $J$ = 8.3 Hz, 1H), 5.95 (dd, $J$ = 7.9, 1.4 Hz, 1H). MALDI-TOF m/z:

$[M]^+$ Calculated for $C_{32}H_{19}NO_3$, 465.14; found, 465.51.

**Synthesis of 3-(4-(10*H*-phenoxazin-10-yl)phenyl)phenanthrene-9,10-dione (PhO-PhPXZ).** Using a similar synthesis procedure for PhO-PXZPh with M2 instead of M1 (963 mg, 69%). $^1$H NMR (400 MHz, Chloroform-*d*) δ 8.38-8.23 (m, 3H), 8.17 (d, *J* = 8.0 Hz, 1H), 7.94 (d, *J* = 8.2 Hz, 2H), 7.77 (t, *J* = 8.3 Hz, 2H), 7.53 (t, *J* = 7.2 Hz, 3H), 6.99 (s, 1H), 6.68 (d, *J* = 43.8 Hz, 5H), 6.00 (s, 2H). MALDI-TOF m/z: $[M]^+$ Calculated for $C_{32}H_{19}NO_3$, 465.14; found, 465.03.

**Synthesis of 3-(11,12-di(pyridin-3-yl)dibenzo[*a*,*c*]phenazin-3-yl)-10-phenyl-10*H*-phenoxazine (DPDPZ-PXZPh).** PhO-PXZPh (465 mg, 1 mmol), 4,5-di(pyridin-3-yl) benzene-1,2-diamine (288 mg, 1 mmol) and 30 mL AcOH were added into a round-bottom flask (100 mL) under $N_2$. Then, the mixture solution was refluxed for 12 h at 120 °C. After the reaction was completed, water was added to the mixture, the organic layer was separated to obtain a solid residue, and the crude product was further purified by column chromatography to obtain the product (553 mg, 80%). $^1$H NMR (400 MHz, Chloroform-*d*) δ 9.33 (dd, *J* = 21.5, 8.2 Hz, 2H), 8.62 (d, *J* = 25.5 Hz, 6H), 8.38 (d, *J* = 2.4 Hz, 2H), 7.78 (dt, *J* = 26.1, 7.6 Hz, 3H), 7.68 – 7.50 (m, 5H), 7.41 (d, *J* = 7.0 Hz, 2H), 7.29 (s, 2H), 7.16 (d, *J* = 2.1 Hz, 1H), 7.05 (dd, *J* = 8.3, 2.1 Hz, 1H), 6.77 – 6.61 (m, 3H), 6.04 (d, *J* = 8.2 Hz, 1H), 5.96 (d, *J* = 7.9 Hz, 1H). $^{13}$C NMR (101 MHz, $CDCl_3$, δ) 150.43, 148.77, 144.33, 143.76, 143.40, 143.31, 142.04, 141.62, 141.37, 138.97, 138.80, 138.68, 137.23, 135.65, 134.45, 133.93, 133.49, 132.44, 132.21, 131.20, 131.14, 130.70, 130.65, 130.21, 128.76, 128.48, 128.09, 126.90, 126.44, 126.02, 123.44, 123.01, 122.94, 122.10, 121.66, 120.13, 115.53, 114.05, 113.58, 113.46. MALDI-TOF m/z: $[M]^+$ Calculated for $C_{48}H_{29}N_5O$, 691.24; found, 691.15. Elemental analysis (%) for $C_{48}H_{29}N_5O$: C 83.34, H 4.23, N 10.12; found: C 83.31, H 4.24, N 10.14.

**Synthesis of 10-(4-(11,12-di(pyridin-3-yl)dibenzo[*a*,*c*]phenazin-3-yl)phenyl)-10*H*-phenoxazine (DPDPZ-PhPXZ).** Using a similar synthesis procedure for DPDPZ-

PhPXZ with PhO-PXZPh instead of PhO-PhPXZ (518 mg, 75%). $^{1}$H NMR (400 MHz, Chloroform-*d*) δ 8.38 – 8.23 (m, 3H), 8.17 (d, *J* = 8.0 Hz, 1H), 7.94 (d, *J* = 8.2 Hz, 2H), 7.77 (t, *J* = 8.3 Hz, 2H), 7.53 (t, *J* = 7.2 Hz, 3H), 6.99 (s, 1H), 6.68 (d, *J* = 43.8 Hz, 5H), 6.00 (s, 2H). $^{13}$C NMR (101 MHz, $CDCl_3$, δ) 150.43, 148.87, 144.03, 143.55, 143.23, 142.38, 141.69, 141.63, 140.95, 139.27, 139.23, 138.91, 137.23, 135.60, 134.33, 132.71, 132.12, 131.50, 131.28, 131.21, 130.83, 130.37, 130.16, 129.43, 128.42, 127.25, 127.10, 126.60, 123.32, 123.05, 121.75, 121.50, 115.57, 113.33. MALDI-TOF m/z: $[M]^+$ Calculated for $C_{48}H_{29}N_5O$, 691.24; found, 691.17. Elemental analysis (%) for $C_{48}H_{29}N_5O$: C 83.34, H 4.23, N 10.12; found: C 83.35, H 4.26, N 10.13.

## Thermal Stability

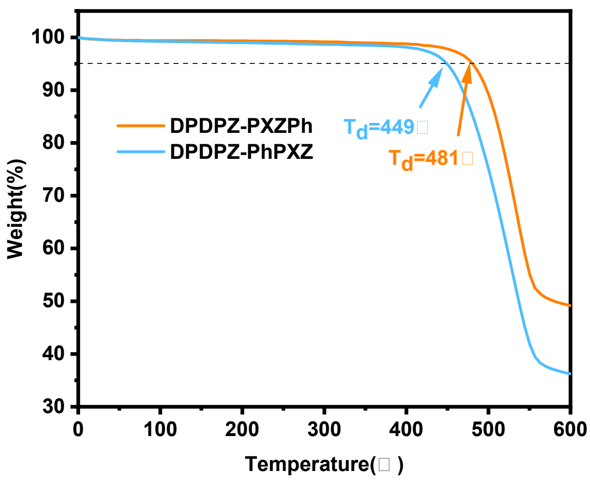


**Figure S1.** TGA curves of DPDPZ-PXZPh and DPDPZ-PhPXZ.

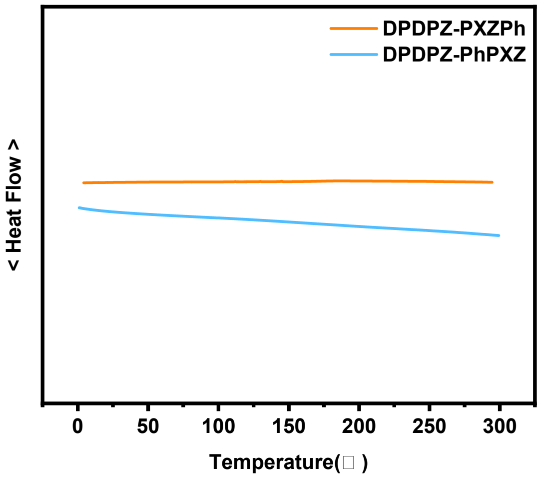


**Figure S2.** DSC curves of DPDPZ-PXZPh and DPDPZ-PhPXZ with a heating rate of 10 °C min$^{-1}$ under $N_2$.

## Theoretical Calculations

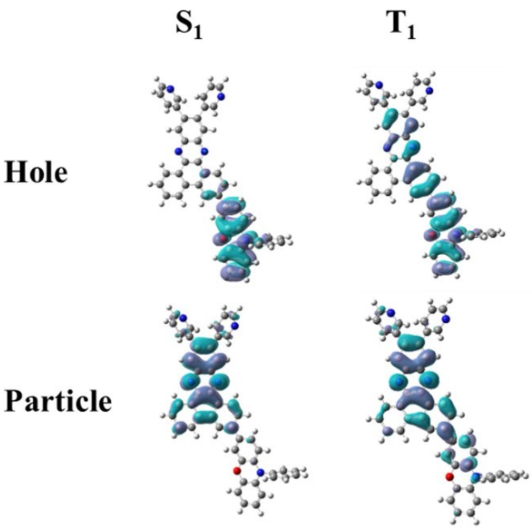


**Figure S3.** Natural transition orbitals (NTOs) of singlet ($S_1$) and triplet ($T_1$) excited states of DPDPZ-PXZPh.

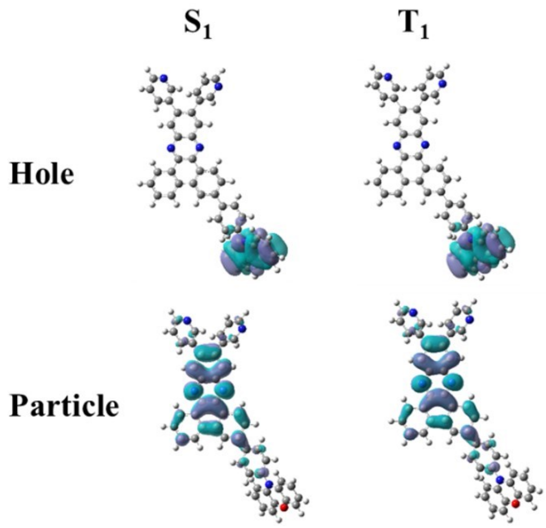


**Figure S4**. Natural transition orbitals (NTOs) of singlet (S1) and triplet (T1) excited states of DPDPZ-PhPXZ.

## Electrochemical Measurement

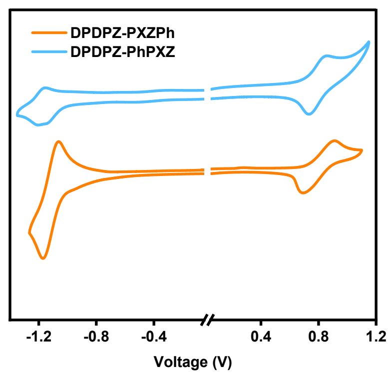


**Figure S5.** Cyclic voltammogram curves of DPDPZ-PXZPh and DPDPZ-PhPXZ.

## Photophysical Properties

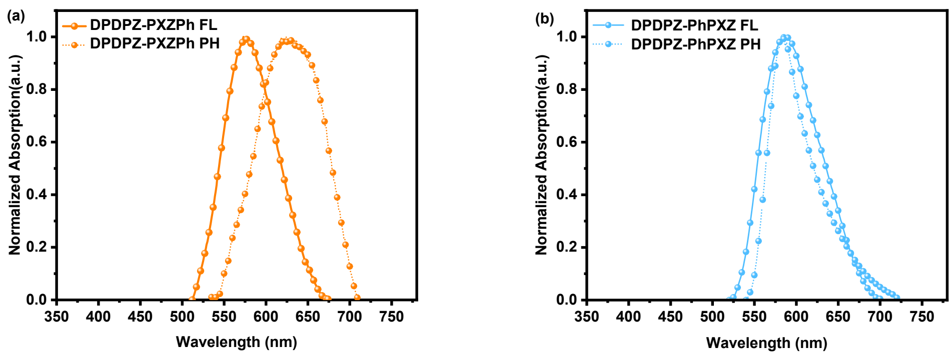


**Figure S6.** Normalized low-temperature fluorescence and phosphorescence spectra measured at 77 K of 7 wt% (a) DPDPZ-PXZPh and (b) DPDPZ-PhPXZ doped in the CBP thin films.

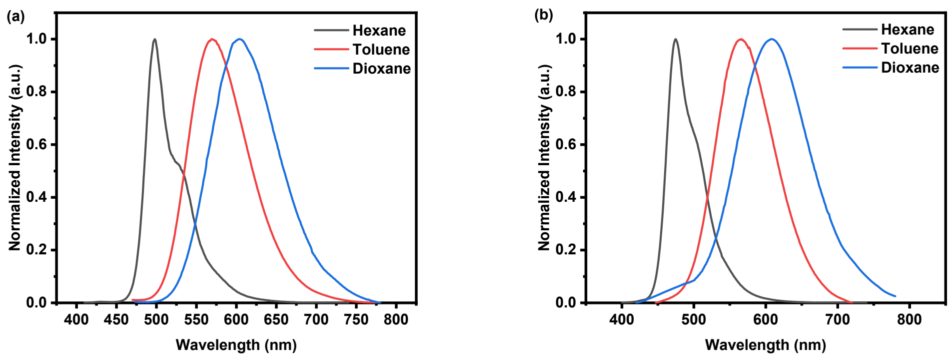


**Figure S7** Normalized PL spectra of (a) DPDPZ-PXZPh and (b) DPDPZ-PhPXZ in various solvents with different polarities.

## Transient PL Measurements

The key kinetic parameters of DPDPZ-PXZPh- and DPDPZ-PhPXZ-doped films are calculated according to the following equations[2]:

$$k_p = \frac{1}{\tau_p} \qquad (1)$$

$$k_d = \frac{1}{\tau_d} \qquad (2)$$

$$k_r^s = k_p \phi_p \qquad (3)$$

$$k_{ISC} = k_p(1 - \phi_p) \qquad (4)$$

$$k_{RISC} = \frac{k_p k_d \phi_d}{k_{ISC} \phi_p} \quad (5)$$

$$\phi_p = \frac{k_r}{k_r + k_{IC}} \quad (6)$$

where $\tau_p$ and $\tau_d$ represent the prompt and delayed decay lifetimes, respectively; $\phi$, $\phi_p$ and $\phi_d$ are the total, prompt and delayed fluorescence quantum efficiencies, respectively; $k_p$, $k_{RISC}$, and $k_d$ are the rate constants of prompt fluorescence, RISC, and delayed fluorescence decay, respectively; and $k_{IC}$ is the internal conversion rate from $S_1$ to $S_0$. The key kinetic parameters are summarized in **Table S1**.

**Table S1.** Kinetic parameters of DPDPZ-PXZPh and DPDPZ-PhPXZ

| EMLs | $\phi_{PL}$ [a] [%] | $\phi_p$ [b] [%] | $\phi_d$ [b] [%] | $\tau_p$ [ns] | $\tau_d$ [μs] | $k_r^S$ [$10^7$ s$^{-1}$] | $k_P$ [$10^7$ s$^{-1}$] | $k_d$ [$10^4$ s$^{-1}$] | $k_{ISC}$ [$10^7$ s$^{-1}$] | $k_{RISC}$ [$10^4$ s$^{-1}$] | $k_{IC}$ [$10^6$ s$^{-1}$] |
|---|---|---|---|---|---|---|---|---|---|---|---|
| DPDPZ-PXZPh | 95 | 68 | 27 | 11.64 | 397.80 | 5.81 | 8.59 | 0.25 | 2.78 | 0.31 | 3.06 |
| DPDPZ-PhPXZ | 68 | 30 | 38 | 32.68 | 15.43 | 0.93 | 3.06 | 6.48 | 2.13 | 11.50 | 4.39 |

(a) Absolute PL quantum yields evaluated by using an integrating sphere of 7 wt% DPDPZ-PXZPh and DPDPZ-PhPXZ doped in CBP host under nitrogen conditions; (b) Determined from the ratio of prompt ($r_1$) and delayed ($r_2$) components in transient decay.

## Electroluminescence Properties

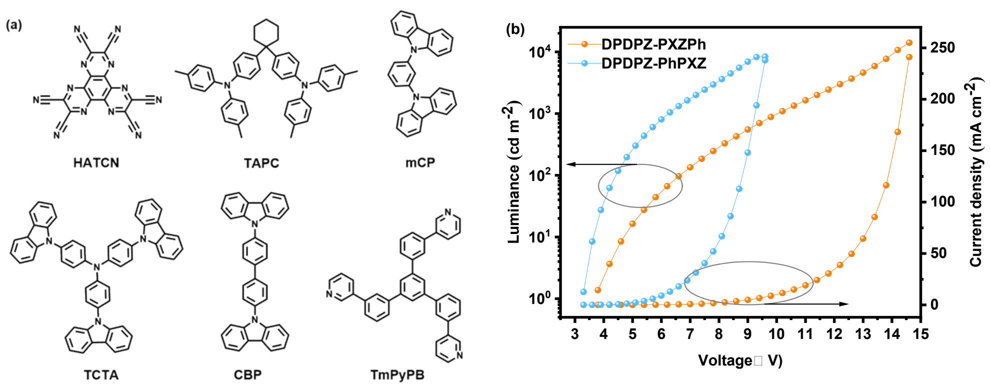


**Figure S8.** (a) Chemical structures of materials used in the OLEDs; (b) Luminance-voltage-current density characteristics of the OLEDs at an optimal doping concentration of 7 wt%.

**Table S2.** EL performances of representative orange-red and red TADF emitters containing dibenzo[*a*,*c*]phenazine acceptor cores in the range of 560-640 nm.

| Emitters | EL (nm) | CE (cd $A^{-1}$) | PE (lm $W^{-1}$) | EQE (%) | CIE (x, y) | References |
|---|---|---|---|---|---|---|
| DPDPZ-PXZPh | 600 | 54.4 | 40.7 | 28.0 | (0.57, 0.43) | This work |
| APZ | 562 | 87.0 | 97.7 | 27.5 | (0.44, 0.55) | 3 |
| TNPZ | 582 | 50.0 | 49.1 | 18.3 | (0.53, 0.47) | 4 |
| 2SPAC-DBP-2tBuCz | 583 | 38.6 | 48.8 | 23.7 | (0.54, 0.45) | 5 |
| 2DMAC-DBP-2tBuCz | 606 | 34.7 | 44.7 | 18.9 | (0.57, 0.42) | |
| 1PXZ-BP | 590 | 47.2 | 57.1 | 26.3 | (0.52, 0.46) | 6 |
| 2PXZ-BP | 606 | 27.4 | 33.1 | 19.2 | (0.57, 0.42) | |
| DPPM-DMAC | 596 | 47.9 | 47.0 | 23.1 | (0.56, 0.44) | 7 |
| (R)-ODPPXZ | 600 | 41.7 | 43.9 | 20.3 | (0.53, 0.45) | 8 |
| TAT-DBPZ | 604 | 29.7 | 23.3 | 15.4 | (0.61, 0.38) | 9 |
| 3DMAC-BP | 606 | 38.2 | 36.4 | 22.0 | (0.58, 0.41) | 10 |
| BPSPXZ | 623 | 16.3 | 17.1 | 15.8 | (0.62, 0.37) | 11 |

## NMR Spectra

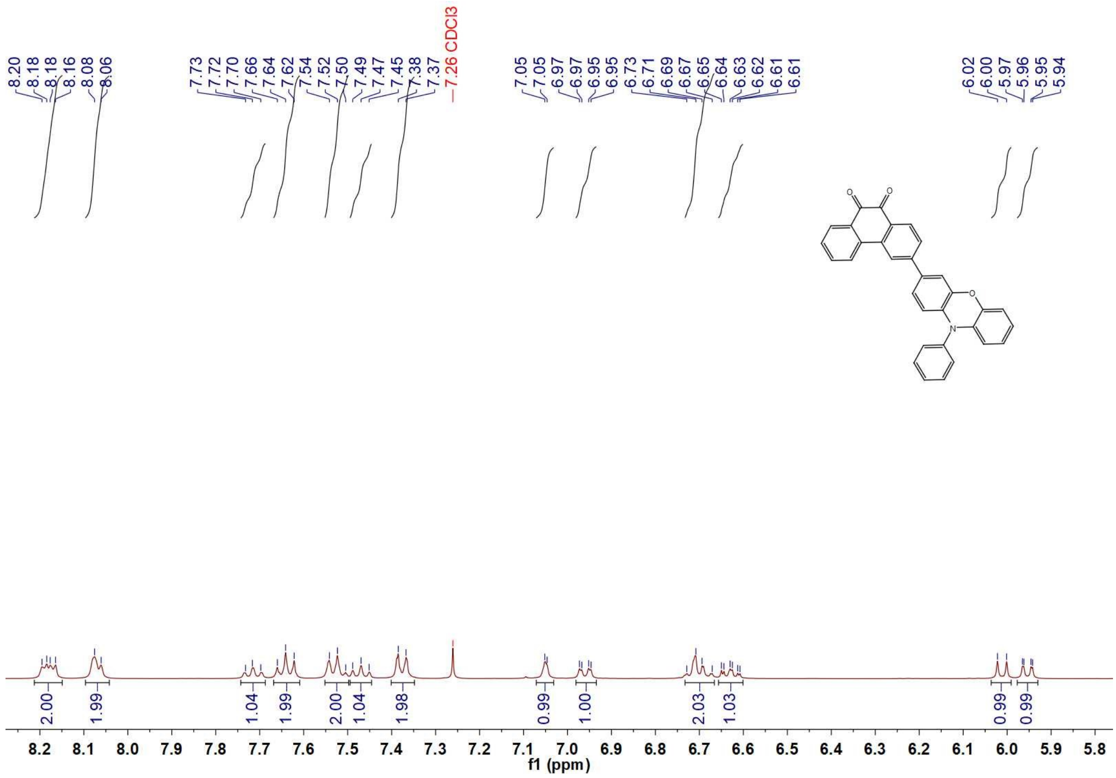

**Figure S9**. $^{1}H$ NMR spectrum ($CDCl_3$, 400 MHz) of PhO-PXZPh.

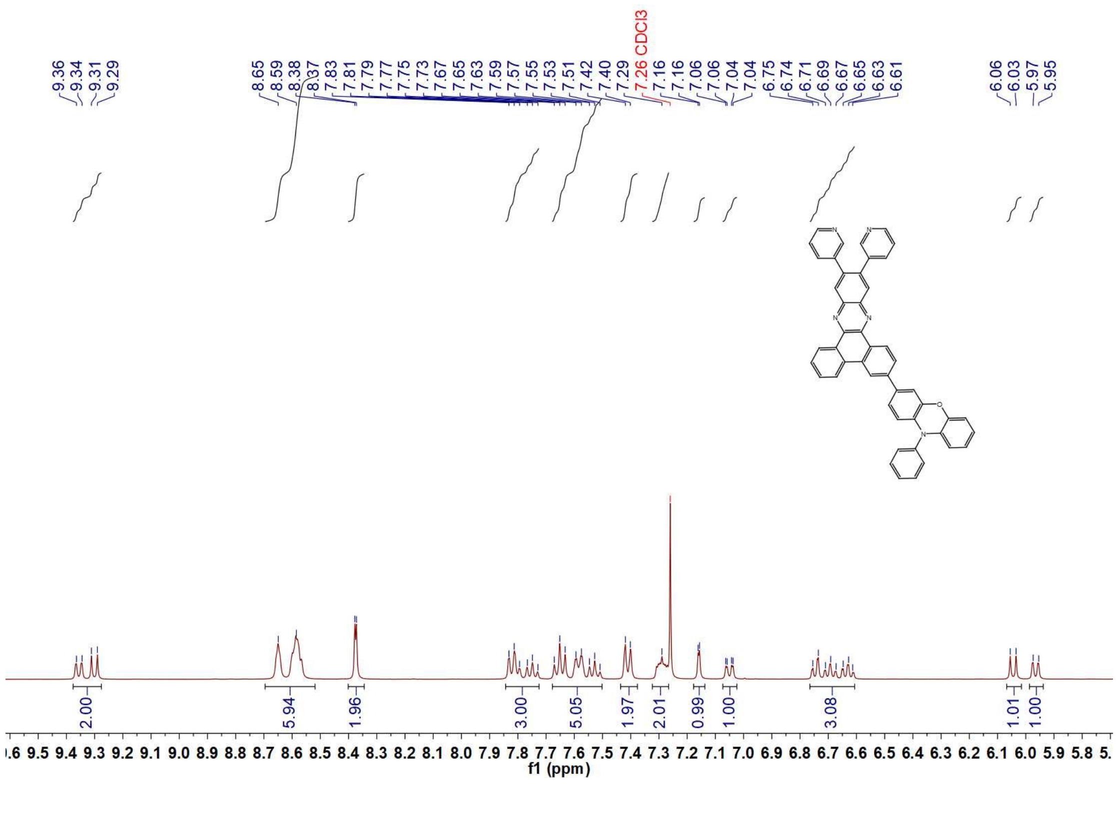

**Figure S10**. $^{1}H$ NMR spectrum ($CDCl_3$, 400 MHz) of DPDPZ-PXZPh.

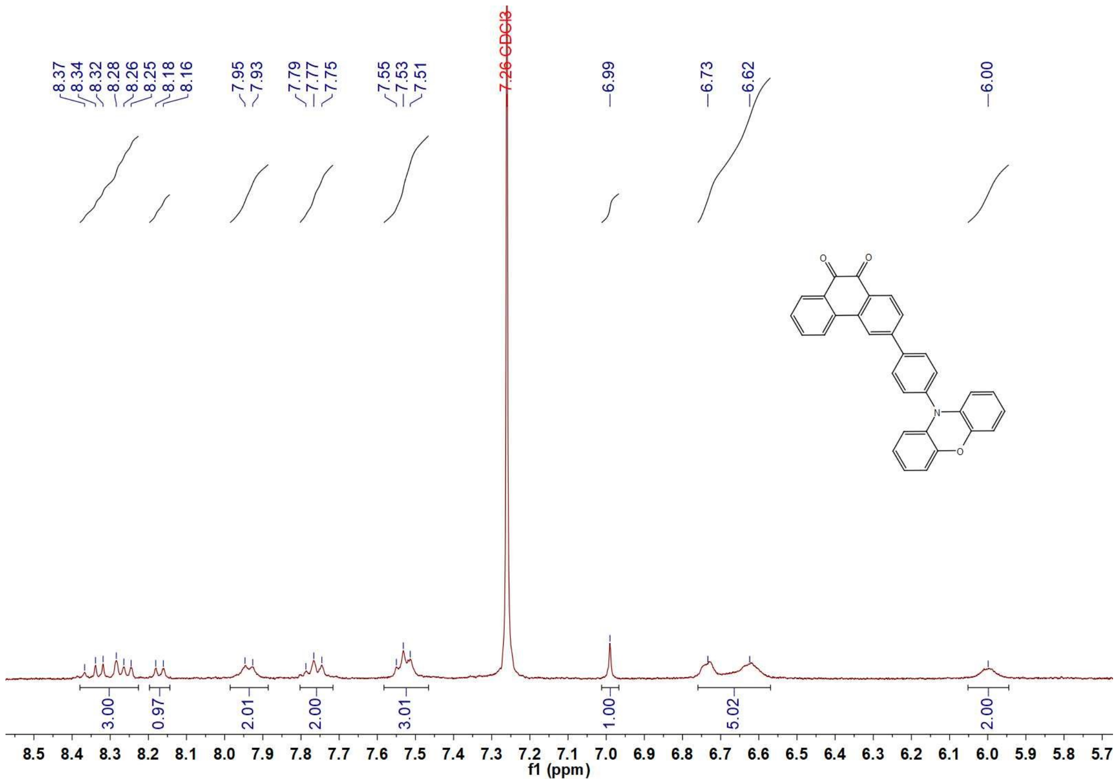


**Figure S11**. $^{1}H$ NMR spectrum ($CDCl_3$, 400 MHz) of PhO-PhPXZ.

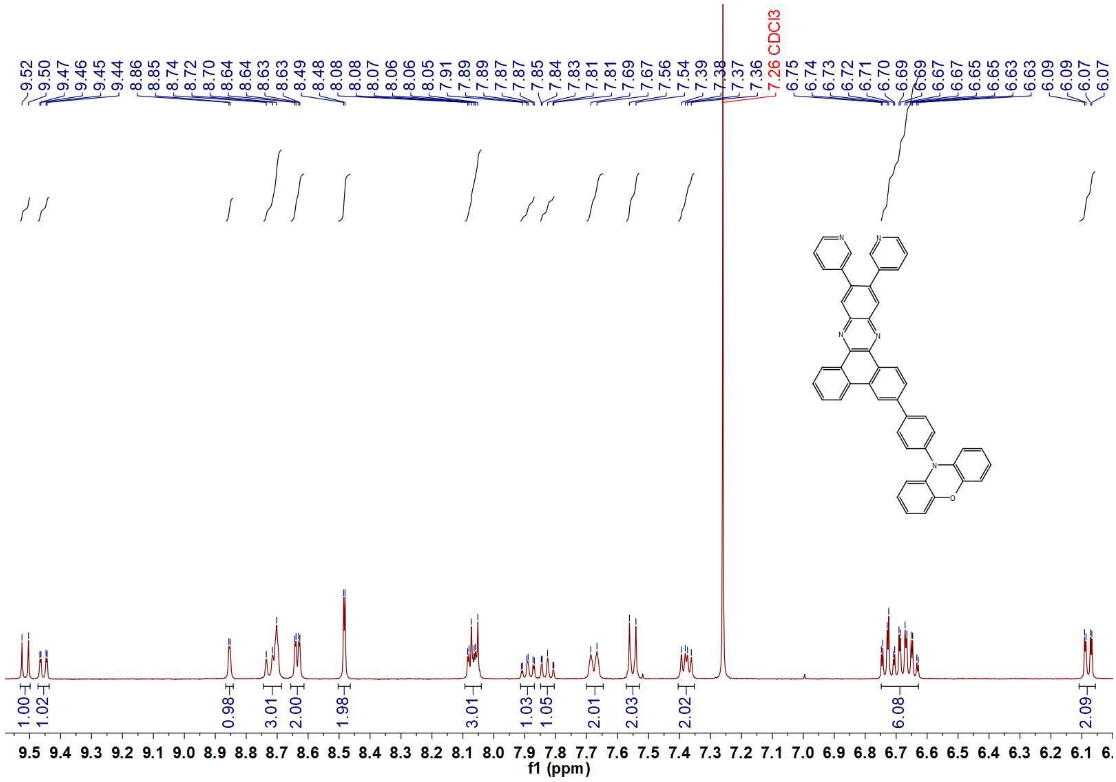


**Figure S12**. $^{1}H$ NMR spectrum ($CDCl_3$, 400 MHz) of DPDPZ-PhPXZ.

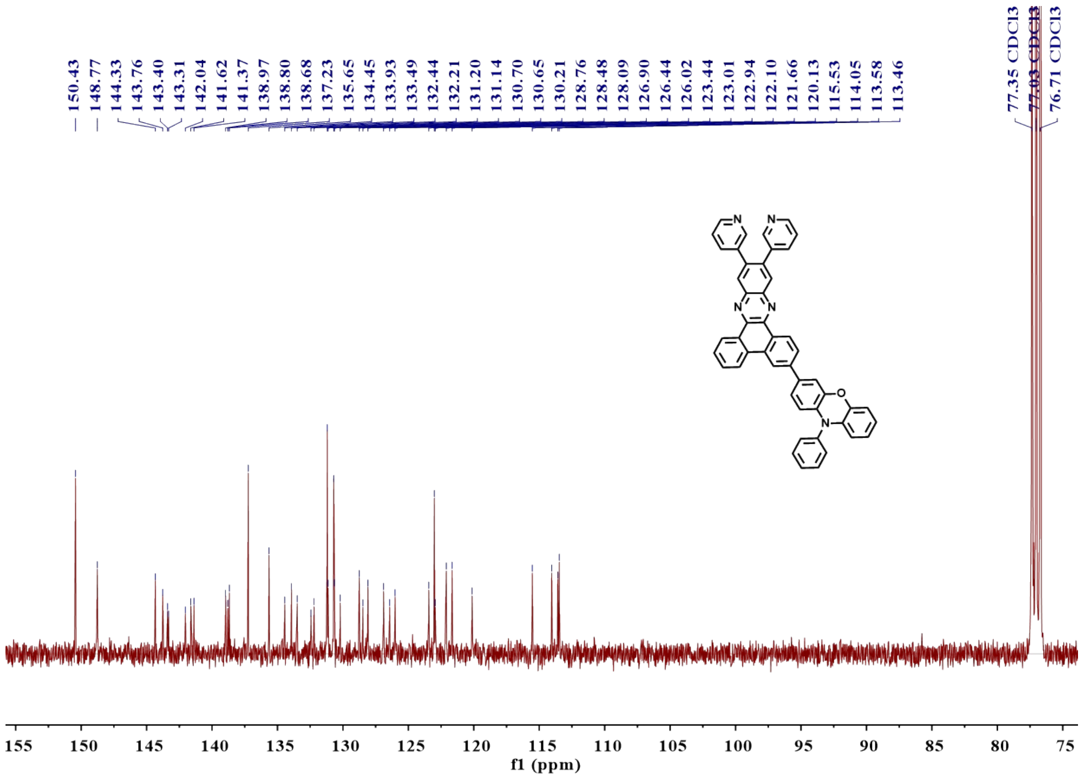

**Figure S13**. $^{13}C$ NMR spectrum ($CDCl_3$, 400 MHz) of DPDPZ-PXZPh.

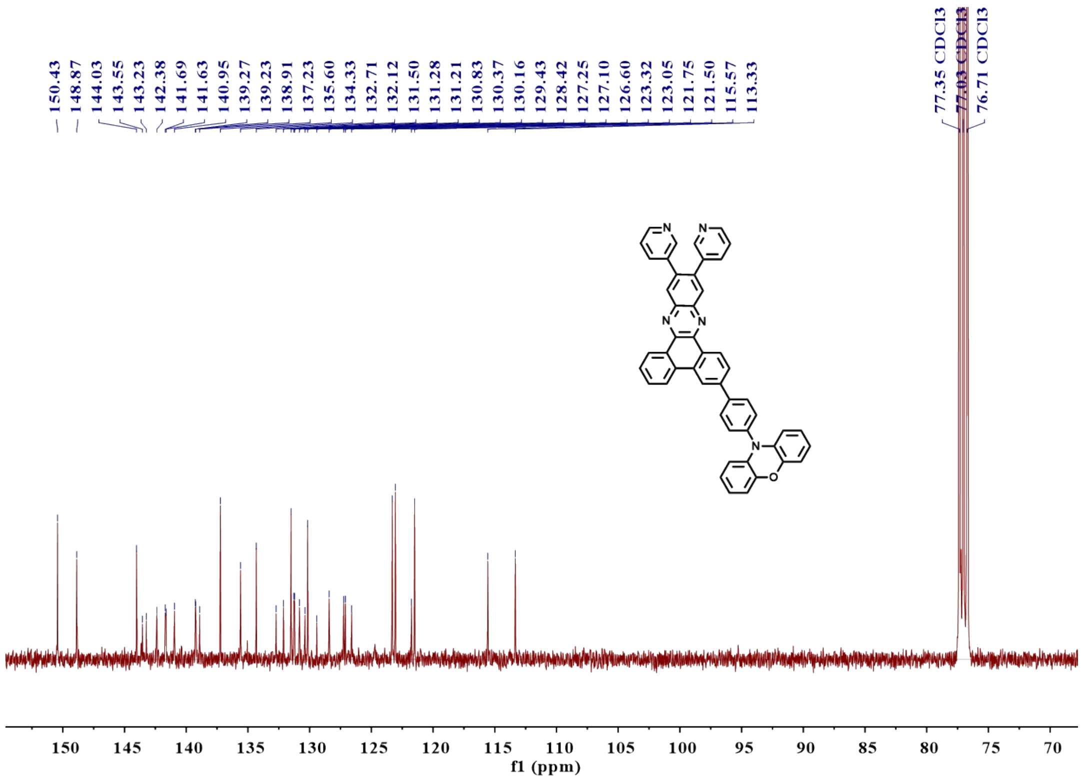

**Figure S14**. $^{13}C$ NMR spectrum ($CDCl_3$, 400 MHz) of DPDPZ-PhPXZ.

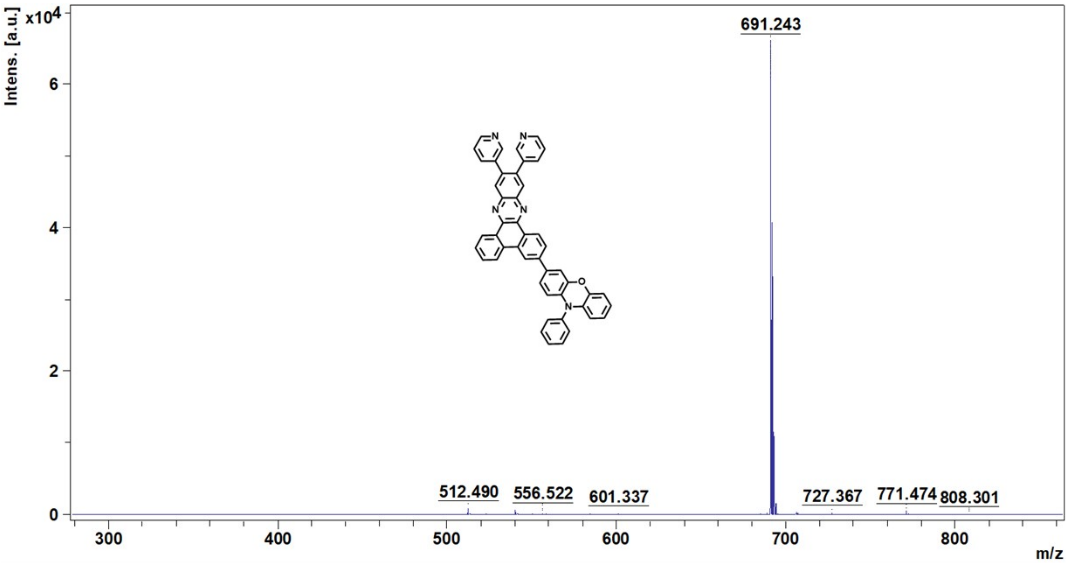


**Figure S15**. MALDI-TOF mass spectrum of DPDPZ-PXZPh.

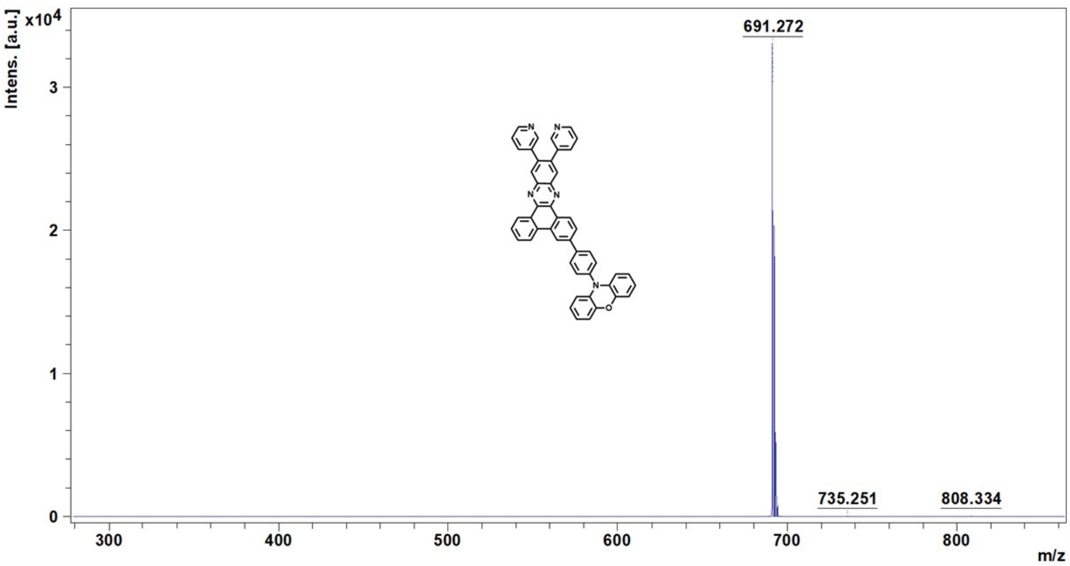


**Figure S16**. MALDI-TOF mass spectrum of DPDPZ-PhPXZ.

## References


1 C. Wang, X. L. Li, Y. Gao, L. Wang, S. Zhang, L. Zhao, P. Lu, B. Yang, S. J. Su, Y. Ma, Efficient near-Infrared (NIR) Organic Light-Emitting Diodes Based on Donor-Acceptor Architecture: An Improved Emissive State from Mixing to Hybridization, *Adv. Opt. Mater.*, 2017**, 5**, 1700441.

2 Q. Zhang, H. Kuwabara, W.J. Potscavage, Jr., S. Huang, Y. Hatae, T. Shibata, C.

Adachi, Anthraquinone-Based Intramolecular Charge-Transfer Compounds: Computational Molecular Design, Thermally Activated Delayed Fluorescence, and Highly Efficient Red Electroluminescence, *J. Am. Chem. Soc.*, 2014**, 136**, 18070-18081.

3 Y. Liu, J. Yang, Z. Mao, D. Ma, Y. Wang, J. Zhao, S. J. Su, Z. Chi, Donor or Acceptor: Molecular Engineering Based on Dibenzo[*a*,*c*]Phenazine Backbone for Highly Efficient Thermally-Activated Delayed Fluorescence Organic Light-Emitting Diodes, *Adv. Opt. Mater.*, 2022**, 11**, 2201695.

4 Y. Liu, J. Yang, Z. Mao, Y. Wang, J. Zhao, S. J. Su, Z. Chi, Isomeric Thermally Activated Delayed Fluorescence Emitters for Highly Efficient Organic Light-Emitting Diodes, *Chem. Sci.*, 2023**, 14**, 1551-1556.

5 D. Jiang, H. Sasabe, H. Arai, K. Nakao, K. Kumada, J. Kido, Extremely High Power Efficiency Solution-Processed Orange-Red TADF OLEDs Via a Synergistic Strategy of Molecular and Device Engineering, *Adv. Opt. Mater.*, 2022**, 10**, 2102774.

6 F. M. Xie, P. Wu, S. J. Zou, Y. Q. Li, T. Cheng, M. Xie, J. X. Tang, X. Zhao, Efficient Orange-Red Delayed Fluorescence Organic Light-Emitting Diodes with External Quantum Efficiency over 26%, *Adv. Electron. Mater.*, 2019**, 6**, 1900843.

7 R. Jiang, X. Wu, H. Liu, J. Guo, D. Zou, Z. Zhao, B. Z. Tang, High-Performance Orange-Red Organic Light-Emitting Diodes with External Quantum Efficiencies Reaching 33.5% Based on Carbonyl-Containing Delayed Fluorescence Molecules, *Adv. Sci.*, 2022**, 9**, e2104435.

8 F. M. Xie, J. X. Zhou, X. Y. Zeng, Z. D. An, Y. Q. Li, D. X. Han, P. F. Duan, Z. G. Wu, Y. X. Zheng, J. X. Tang, Efficient Circularly Polarized Electroluminescence from Chiral Thermally Activated Delayed Fluorescence Emitters Featuring Symmetrical and Rigid Coplanar Acceptors, *Adv. Opt. Mater*., 2021**, 9,** 2100017.

9 Y. Liu, Y. Chen, H. Li, S. Wang, X. Wu, H. Tong, L. Wang, High-Performance Solution-Processed Red Thermally Activated Delayed Fluorescence OLEDs Employing Aggregation-Induced Emission-Active Triazatruxene-Based Emitters, *ACS Appl. Mater. Interfaces*, 2020**, 12**, 30652-30658.

10 F. M. Xie, H. Z. Li, G. L. Dai, Y. Q. Li, T. Cheng, M. Xie, J. X. Tang, X. Zhao, Rational Molecular Design of Dibenzo[*a*,*c*]Phenazine-Based Thermally Activated Delayed Fluorescence Emitters for Orange-Red OLEDs with EQE up to 22.0%, *ACS Appl. Mater. Interfaces*, 2019**, 11**, 26144-26151.

11 J. X. Chen, H. Wang, Y. F. Xiao, K. Wang, M. H. Zheng, W. C. Chen, L. Zhou, D. Hu, Y. Huo, C. S. Lee, X. H. Zhang, Optimizing Intermolecular Interactions and Energy Level Alignments of Red TADF Emitters for High-Performance Organic Light-Emitting Diodes, *Small*, 2022**, 18**, e2201548.